Charge radii and neutron correlations in helium halo nuclei

G. Papadimitriou, A. T. Kruppa, N. Michel, W. Nazarewicz, M. Płoszajczak, and J. Rotureau

Phys. Rev. C **84**, 051304 — Published 10 November 2011

DOI: 10.1103/PhysRevC.84.051304

Charge radii and neutron correlations in helium halo nuclei

G. Papadimitriou,[1,2] A.T. Kruppa,[1,3] N. Michel,[4] W. Nazarewicz,[1,2,5] M. Płoszajczak,[6] and J.Rotureau[7]

[1] *Department of Physics and Astronomy, University of Tennessee, Knoxville, Tennessee 37996, USA*
[2] *Physics Division, Oak Ridge National Laboratory, Oak Ridge, Tennessee 37831, USA*
[3] *Institute of Nuclear Research, P.O. Box 51, H-4001 Debrecen, Hungary*
[4] *Department of Physics, Post Office Box 35 (YFL), FI-40014 University of Jyväskylä, Finland*
[5] *Institute of Theoretical Physics, University of Warsaw, ul. Hoża 69, PL-00-681 Warsaw, Poland*
[6] *Grand Accélérateur National d'Ions Lourds (GANIL), CEA/DSM-CNRS/IN2P3, BP 55027, F-14076 Caen Cedex, France*
[7] *Department of Physics, University of Arizona, Tucson, Arizona 85721, USA*

Within the complex-energy configuration interaction framework, we study correlations of valence neutrons to explain the behavior of charge radii in the neutron halo nuclei ^{6,8}He. We find that the experimentally observed decrease of the charge radius between ^{6}He and ^{8}He is caused by a subtle interplay between three effects: dineutron correlations, a spin-orbit contribution to the charge radius, and a core swelling effect. We demonstrate that two-neutron angular correlations in the 2^+_1 resonance of ^{6}He differ markedly from the ground-state correlations in ^{6,8}He. Finally, we discuss the impact of the neutron threshold position and valence neutron correlation energy on the neutron radius, i.e., the pairing-antihalo effect.

PACS numbers: 21.10.Gv,21.10.Ft,21.60.Cs,27.20.+n

Introduction—The physics of Open Quantum Systems (OQS) [1] has attracted a lot of attention in many fields of physics, including atomic and molecular physics, quantum optics, condensed matter physics, nuclear physics, and tests of quantum mechanics. In atomic nuclei, the "openness" of the system manifests itself by the coupling to the many-body continuum representing various decay and reaction channels [2, 3]. In addition to being prototypical OQSs, nuclei are excellent laboratories of many-body physics. While the number of fermions in nuclei is very small compared to atoms, molecules, and solids, nuclei exhibit an emergent behavior that is present in other complex systems. Due to the presence of particle thresholds, atomic nuclei form a network of correlated fermionic systems interconnected via reaction channels. The effects due to openness are enhanced in weakly bound nuclei [4]. Indeed, an essential part of the motion of those short-lived systems, such as extended nuclear halos, is in classically forbidden regions, and their properties are profoundly impacted by both the continuum and many-body correlations.

The neutron-rich helium isotopes ^{6}He and ^{8}He, which are subjects of this study, are excellent representatives of OQS. Indeed, both nuclei are Borromean halos, they have no bound excited states, and they exhibit the binding-energy anomaly, i.e., the presence of higher one- and two-neutron emission thresholds in ^{8}He than in ^{6}He. Studies of charge radii of nuclear halos represent a splendid example of the cross-fertilization between atomic and nuclear physics in the field of OQSs. Experimentally, charge radii of helium halos were extracted from measured isotopic shifts of helium atoms in pioneering studies of Refs. [5, 6]. Very recently, these numbers were revaluated [7] based on precision mass measurements. It was found that the charge radius of ^{6}He, 2.059(7) fm, exceeds that of ^{8}He, 1.959(16) fm, and both radii are much larger than the charge radius of ^{4}He (1.681(4) fm [8]). Since the charged protons are confined inside the tightly bound α-core, the differences of charge radii of helium halos carry unique structural information on nuclear Hamiltonians and nuclear many-body dynamics.

Because of their precision, charge radius data provide a critical test of nuclear models. Charge radii have been calculated successfully within the *ab initio* GFMC [9] and NCSM [10] frameworks using state-of-the-art realistic interactions. However, not much is known about the particle correlations that cause this behavior. To obtain a simple physical picture of the observed effect and understand the physics that governs the neutron distributions in helium halos, in this Letter, we employ the complex-energy continuum shell model [3], the Gamow Shell Model (GSM) [11]. GSM is a configuration interaction approach with a single-particle (s.p.) basis given by the Berggren ensemble [12], which consists of Gamow (bound and resonance) states and the nonresonant scattering continuum. One can find successful applications of the Berggren ensemble to the helium halos in the earlier GSM calculations [11, 13, 14] and also in *ab initio* coupled-cluster calculations of Ref. [15]. Since the dynamics of halo neutrons in ^{6,8}He is primarily governed by many-body correlations and continuum coupling, GSM is the tool of choice to get a simple insight into underlying physics.

Model—We assume that the halo nucleus can be described as a system of n_ν valence neutrons moving around a closed ^{4}He core. To cope with the problem of spurious center-of-mass motion, we adopt a system of intrinsic nucleon-core coordinates inspired by the cluster orbital shell model [16]. In these coordinates, the translationally invariant GSM Hamiltonian is: $H = \sum_{i=1}^{n_\nu}\left[\frac{p_i^2}{2\mu}+U_i\right] + \sum_{i<j}^{n_\nu}\left[V_{ij}+\frac{1}{A_c m_N}\boldsymbol{p}_i\boldsymbol{p}_j\right]$, where U_i is the single-particle

(s.p.) potential describing the field of the core, V_{ij} is the two-body residual interaction between valence neutrons, and the last term represents the two-body energy recoil with $A_c = 4$. For the one-body potential, we took the "^{5}He" Woods-Saxon (WS) field (with spin-orbit term) of Ref. [11] which reproduces the experimental energies and widths of known s.p. $3/2^-$ and $1/2^-$ resonances in ^{5}He. The residual interaction employed is a finite-range Minnesota (MN) central potential [17], which is a sum of three Gaussians with different ranges. Since only a T=1 interaction channel is present, two Gaussians are sufficient; this has been achieved by taking the parameter u=1 of the original MN potential [17]. As the interaction coupling constants should depend on the configuration space used, in our work we alter the Gaussian strengths V_{0R} and V_{0s} of the MN potential to reproduce the experimental ground state (g.s.) energies of ^{6,8}He ($V_{0R} = 250.2\,\mathrm{MeV}$ and $V_{0s} = -110.1\,\mathrm{MeV}$); the Gaussian ranges are the same as in Ref. [17]. The one-body basis is given by the Berggren ensemble, which for the case of ^{6}He is that of the "^{5}He" WS field. For the heavier helium isotopes, the quality of the WS basis deteriorates; hence, we use a Gamow Hartree-Fock (GHF) ensemble [18] generated by the WS potential and the modified MN interaction. The two-body matrix elements of V_{ij} and the recoil term are efficiently computed by using the Harmonic Oscillator (HO) expansion method [13, 14]. This requires calculating the overlaps between Berggren basis and HO states. Because of the Gaussian asymptotic behavior of HO wave functions, no complex scaling is needed, since these overlaps always converge. By taking the HO length parameter b=2 fm and the lowest 16 HO states for each partial wave, we obtain full convergence and perfect agreement with the Complex Scaling (CS) approach in the Slater basis [19]. The calculations were carried out in a large shell model space consisting of the $0p_{3/2}$ Gamow resonance and non-resonant *psd* scattering continua. The maximum s.p. momentum was chosen to be $k_{max} = 4.0\,\mathrm{fm}^{-1}$. The $p_{3/2}$ contour in the complex momentum plane was discretized with a total of 30 points, while the remaining non-resonant continua were chosen along the real momentum axis and discretized with 21 points each; this resulted in a large GSM space of 115 shells. In this space, the dimension of the GSM Hamiltonian matrix for the ^{8}He becomes prohibitively large, and, for this reason, we applied the Density Matrix Renormalization Group approach earlier adopted to GSM in Refs. [20]. Since the s-wave enters the Berggren ensemble, in order to satisfy the Pauli Principle between core and valence particles we apply the Saito's Orthogonality Condition Model [21].

Radii and neutron correlations—To obtain the charge radii of ^{6,8}He we first express the proton point radius in the intrinsic set of coordinates: $\langle r^2_{pp}(^{A_c+n_\nu}X)\rangle = \langle r^2_{pp}(^{A_c}X)\rangle + \frac{1}{(A_c+n_\nu)^2}\sum_{i=1}^{n_\nu}\langle r_i^2\rangle + \frac{2}{(A_c+n_\nu)^2}\sum_{i<j}^{n_\nu}\langle \boldsymbol{r}_i\cdot\boldsymbol{r}_j\rangle$, where the first term is the point proton radius of the α-core in nucleus $^{A_c+n_\nu}X$, and the two remaining terms represent the contribution to the proton radius from the motion of the core around the nuclear center-of-mass, i.e., recoil effect. The *ab initio* GFMC calculations [22] predict the 4.58% and 6.66% increase of the α-particle proton point radius in ^{6}He and ^{8}He, respectively. (The effect of core polarization by valence neutrons cannot be totally decoupled from the effect of $\boldsymbol{\tau}\cdot\boldsymbol{\tau}$ forces, which virtually exchange protons with neutrons.) By assuming these numbers, together with the experimental value of 1.46 fm for the α-particle point radius, we adopt the point proton radius of 1.527 fm (1.557 fm) for ^{6}He (^{8}He). This core "swelling" effect due to valence neutrons is large enough that it cannot be neglected in the detailed analysis. To make contact with the measured charge radii, we correct the calculated point-proton radii for the finite sizes of proton and neutron through the usual expression [23]: $\langle r^2_{ch}\rangle = \langle r^2_{pp}\rangle + \langle R^2_p\rangle + \frac{N}{Z}\langle R^2_n\rangle + \frac{3}{4M_p^2} + \langle r^2\rangle_{so}$, where $\langle R^2_p\rangle = 0.769\,\mathrm{fm}^2$ (proton charge radius), $\langle R^2_n\rangle = -0.1161\,\mathrm{fm}^2$ [24] (neutron charge radius), $\frac{3}{4M_p^2} = 0.033\,\mathrm{fm}^2$ [25] (Darwin-Foldy term), and $\langle r^2\rangle_{so}$ is the spin-orbit (s.o.) contribution.

The correlations amongst the valence neutrons are assessed through the two-body density $\rho_{nn}(r,r',\theta) = \langle\Psi|\delta(r_1-r)\delta(r_2-r')\delta(\theta_{12}-\theta)|\Psi\rangle$, with r_1 (r_2) being the distance between the core and the first (second) neutron and θ_{12} - the opening angle between the two neutrons. The density $\rho_{nn}(r,r',\theta)$ differs from the two-particle density of Refs. [26, 27] by the absence of the Jacobian $8\pi^2 r^2 r'^2 \sin\theta$. Consequently, $\int \rho_{nn}(r,r',\theta)drdr'd\theta = 1$. In practical implementation, $\rho_{nn}(r,r',\theta)$ has been expressed in the LS coupling scheme [27] and benchmarked against CS calculations [19].

Results—The adopted GSM Hamiltonian reproduces the energetics of the isotopic chain $^{5-8}$He, in particular the one-neutron (1n) and two-neutron (2n) thresholds. We predict the 2^+_1 resonance in ^{6}He to have energy 851 keV ($E_{exp} = 822\,\mathrm{keV}$ [28]) and width $\Gamma = 109$ keV ($\Gamma_{exp} = 113\,\mathrm{keV}$). The predicted $3/2^-$ g.s. resonance of ^{7}He has $E = -0.707$ MeV ($E_{exp} = -0.528\,\mathrm{MeV}$).

Before discussing GSM predictions for the charge and neutron radii, we present results for 2n correlations. Figure 1(a) shows the GSM density $\rho_{nn}(r,\theta) = \rho_{nn}(r_1 = r, r_2 = r, \theta)$ for the g.s. of ^{6}He. The density exhibits two peaks [27, 29–31]. One maximum, corresponding to a small opening angle and a large radial extension, represents the dineutron configuration. The second maximum, found in the region of large angles and radially well localized, represents the cigar-like configuration. Similar to Ref. [27], we find that both configurations have a dominant $S = 0$ component in which the two neutrons are in the spin singlet state (see Fig. 1(b)). The amplitude of the $S = 1$ density component shown in Fig. 1(c) is fairly small (13%); this contribution to density has a very broad maximum around $\theta_{12} = 90^\circ$. To illustrate the importance of the continuum coupling for the dominance of the dineutron configuration in ^{6}He, in Fig. 1(d) we plot $\rho_{nn}(r,\theta)$ calculated in the limited $(p_{3/2})^2$ model space. Interestingly, the omission of $p_{1/2}sd$ scattering continua,

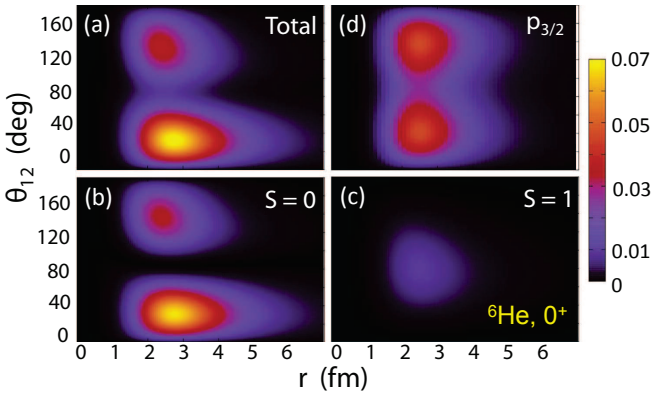

FIG. 1: (Color online) Two-neutron GSM density (in fm^{-2}) of the 0^+ ground state of ^{6}He: (a) total; (b) $S = 0$ component; (c) $S = 1$ component; (d) density in a $p_{3/2}$ model space.

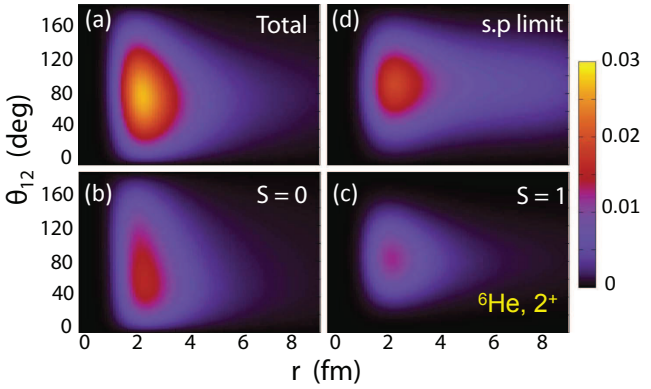

FIG. 2: (Color online) Two-neutron GSM density (in fm^{-2}) of the 2^+_1 resonance in ^{6}He: (a) total; (b) $S = 0$ component; (c) $S = 1$ component; (d) density with the two-body interaction turned off.

which enter the g.s. wave function of ^{6}He with fairly small amplitudes [13], has a rather dramatic effect on 2n distribution: the dineutron component loses its halo character, and the heights of the dineutron and cigar-like peaks become equal.

The unique feature of GSM is that it enables us to examine many-body correlations in unbound states. To this end, we study ρ_{nn} in the 2^+_1 state of ^{6}He, a 2n resonance. As seen in Fig. 2(a), the corresponding 2n density is radially extended, which nicely illustrates the unbound character of the 2^+ state. Contrary to the g.s. density, $\rho_{nn}(r,\theta)$ is characterized by one broad maximum centered around $\theta_{12} = 60°$. We find that the $S = 0$ and $S = 1$ configurations have similar spatial distributions, and the ratio of their amplitudes is ∼2:1. The GSM wave function of the 2^+ resonance is dominated by a $(0p_{3/2})^2$ resonant component [13]. To demonstrate the s.p. character of this state, in Fig. 2(d) we plot $\rho_{nn}(r,\theta)$ obtained by turning the residual interaction off, thus preventing scattering from the $0p_{3/2}$ Gamow state to the non-resonant continua. We see that the resulting density is close to that in the full space. This result suggests that the valence neutrons in the first excited state of ^{6}He are weakly correlated.

We next study the neutron correlations in g.s. of ^{8}He. Since $\rho_{nn}(r,\theta)$ in ^{6}He and ^{8}He are fairly similar, to better see the difference between these two cases, in Fig. 3 we compare the angular correlation densities $\rho_{nn}(\theta_{12}) = \int dr_1 \int dr_2 \rho_{nn}(r_1, r_2, \theta_{12})$. Our calculations

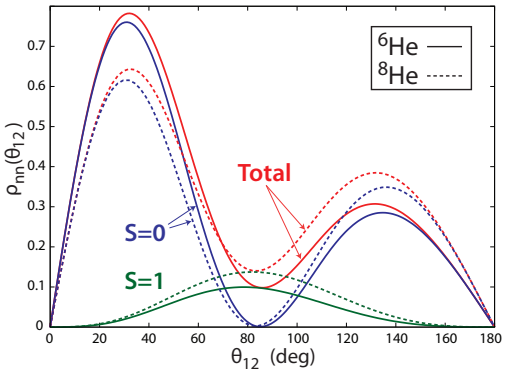

FIG. 3: (Color online) Angular 2n GSM densities (S=0, 1, and total) for g.s. configurations of ^{6}He (solid lines) and ^{8}He (dashed lines).

demonstrate that the weight of the dineutron structure in ^{8}He is less than in ^{6}He due to increased strengths of cigar-like and $S = 1$ components. The addition of the two extra neutrons results in a slight increase in the average opening angle from $\theta_{12} = 68°$ in ^{6}He to $\theta_{12} = 78°$ in ^{8}He. It is worth noting, however, that the positions of the two peaks in $\rho_{nn}(\theta_{12})$ are practically the same in ^{6,8}He, and the 2n correlation density does not broaden up (becomes more "democratic") in ^{8}He. Similar to the case of ^{6}He, the coupling to the non-resonant $p_{1/2}sd$ continua enhances the dineutron configuration in ^{8}He. We carried out calculations in the limited $(p_{3/2})^4$ model space and the resulting 2n correlation density resembles closely that of Fig. 1(d). That is, the heights of the dineutron and cigar-like peaks are equal and the halo character of the dineutron component in ^{8}He is lost.

It has recently been pointed out [33] that $\langle r^2 \rangle_{so}$ may give an appreciable contribution to the charge radii of halo nuclei. We compute the s.o. correction in GSM following Ref. [23]. The calculated s.o. rms radius of ^{6}He (^{8}He) is found to be $\langle r^2 \rangle_{so} = -0.0718 fm^2$ ($-0.158 fm^2$). These values are not very different from s.p. estimates of Ref. [33]; namely, $-0.08 fm^2$ and $-0.17 fm^2$. The final results for charge radii are displayed in Fig. 4: the smaller core recoil and larger s.o. effect in ^{8}He both con-

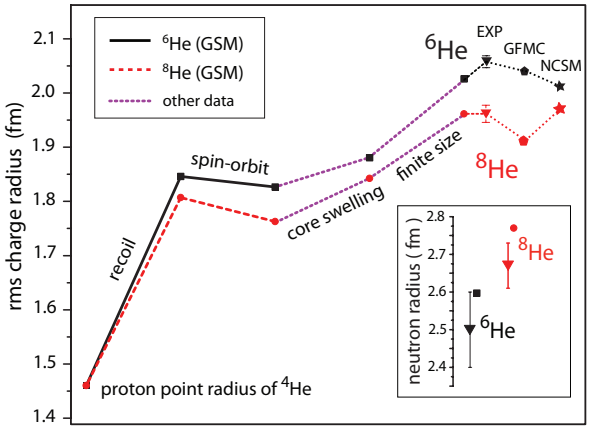

FIG. 4: (Color online) Different contributions to the charge radius of ^{6}He (solid line, squares) and ^{8}He (dashed line, dots) calculated in GSM. The core swelling contribution is taken from GFMC calculations of Ref. [22]. Recently revised experimental charge radii come from [7] (triangles). The NCSM [10] (stars) and GFMC [9] (pentagons) results are marked for comparison. The inset shows GSM rms neutron radii compared to experiment [32].

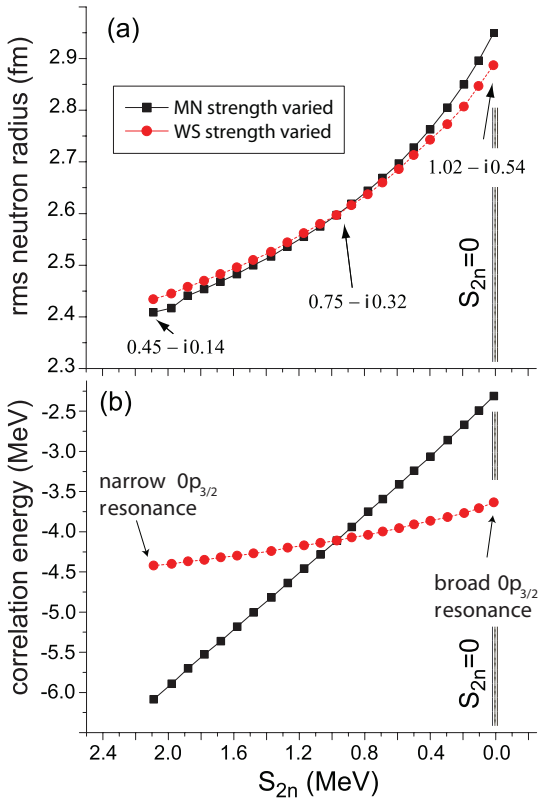

FIG. 5: (Color online) Top: Evolution of the GSM rms neutron radius of ^{6}He as a function of the 2n separation energy S_{2n}. The position of the 2n threshold is varied by (i) changing the strength of the MN interaction (squares) or by (ii) changing the strength of the WS potential (circles). The complex energy $E - i\Gamma/2$ (in MeV) of the $0p_{3/2}$ Gamow resonant state of the WS potential is marked for three values of S_{2n}. Bottom: Correlation energy, i.e., the expectation value of the MN interaction, in the cases (i) and (ii). The 2n threshold $S_{2n} = 0$ is marked by a vertical line.

tribute to the reduced value of $\sqrt{\langle r_{ch}^2 \rangle}$ in this nucleus as compared to ^{6}He. It is to be noted that the recoil effect is primarily sensitive to the 2n threshold energy and the position of the Gamow $0p_{3/2}$ pole [34]. The predicted total values, 2.026 fm for ^{6}He and 1.961 fm for ^{8}He, are in nice agreement with experiment and *ab initio* GFMC and NCSM results. Also, our predicted values of rms neutron radii, shown in the inset of Fig. 4, are consistent with experimental data [32].

It is well known [4] that in the vicinity of the particle threshold pairing correlations can profoundly modify properties of the system. One example is the Pairing-Anti Halo (PAH) effect [35–39], in which pairing correlations in the weakly-bound even-particle system change the asymptotic behavior of particle density thus reducing its radial extension. To assess the sensitivity of the valence neutron extension on the position of the 2n threshold, in Fig. 5 we vary the 2n separation energy S_{2n} of ^{6}He by either changing the V_{0s} singlet strength of the MN interaction that controls the amount of pairing correlations between the valence neutrons (variant 1; V1) or by changing the depth of the WS potential $V_{\rm WS}$ that determines the position of the crucial $0p_{3/2}$ Gamow pole (variant 2; V2). The neutron correlation energy can be estimated by calculating the expectation value of the MN interaction. It is seen in Fig. 5(b) that this quantity strongly depends on V_{0s} in V1 and weakly on $V_{\rm WS}$ in V2. The rms neutron radius of ^{6}He displayed in Fig. 5(a) gradually increases when approaching the 2n threshold $S_{2n} = 0$ in both variants. The faster increase of neutron radius in V1 reflects the more rapid decrease of neutron pairing correlations with S_{2n} in this case. The character of the $0p_{3/2}$ resonance in V2 gradually changes from a moderately narrow one at $S_{2n} = 2\,$MeV to very broad ($\Gamma \approx 1\,$MeV) at $S_{2n} = 0$. In spite of this, the neutron radius gradually approaches the 2n threshold without exhibiting the rapid increase characteristic of an odd-particle halo system [35]. Indeed, in the absence of correlations, the rms radius of the $0p_{3/2}$ state is expected to diverge as $S_{1n}^{-1/2}$ when approaching the threshold [40]. In summary, the result presented in Fig. 5 is a manifestation of the PAH effect in the GSM.

Conclusions—We have applied the translationally invariant GSM with finite-range modified MN interaction to valence neutron correlations, and neutron and charge radii of the halo nuclei ^{6,8}He. Our s.p. basis consists of the $0p_{3/2}$ Gamow resonance and non-resonant *psd* scattering continua resulting in a large configuration space. We obtain good agreement with experiment for charge and neutron rms radii, neutron separation energies in the He chain, and the 2_1^+ resonance in ^{6}He. We find that the charge radii of helium halos depend mainly on three factors: (i) valence neutron correlations resulting in a core

recoil; (ii) s.o. contribution to the charge radius, and (iii) polarization of the core by valence neutrons. We demonstrated that the reduction of the charge radius when going from ^{6}He to ^{8}He is not due to a more "democratic" arrangement of the neutrons around the core but rather due to the reduction of the amplitude of the dineutron configuration in the g.s. wave function, resulting in a smaller core recoil radius. In addition, the negative s.o. radius contribution doubles with the addition of two valence neutrons. The dineutron configuration in ^{6,8}He is strongly enhanced by coupling to the nonresonant continuum. We studied 2n correlations in the 2^+_1 resonance of ^{6}He and found a rather broad distribution characteristic of an uncorrelated s.p. motion with no dineutron component. Finally, we demonstrated the presence of the PAH effect in the rms neutron radius of ^{6}He when approaching the 2n threshold. This is the first evidence for this phenomenon in a configuration-interaction-based framework.

Useful discussions with J. Friar, S. Pieper, and B. Wiringa are gratefully acknowledged. This work was supported by the Office of Nuclear Physics, U.S. Department of Energy under Contract Nos. DE-FG02-96ER40963 (University of Tennessee), DE-FG02-04ER41338 (University of Arizona), and DE-FG02-10ER41700 (French-U.S. Theory Institute for Physics with Exotic Nuclei); by the U.S. NSF under grant PHY-0854912, by the Hungarian OTKA Fund No. K72357; and by the Academy of Finland and University of Jyväskylä within the FIDIPRO programme.

[1] H.-P. Breuer and F. Petruccione. *The Theory of Open Quantum Systems*. Oxford University Press, Oxford, 2002.
[2] J. Okołowicz, M. Płoszajczak, and I. Rotter, Phys. Rep. **374**, 271 (2003).
[3] N. Michel *et al.*, J. Phys. G **36**, 013101 (2009); N. Michel *et al.*, J. Phys. G **37**, 064042 (2010).
[4] J. Dobaczewski *et al.*, Prog. Part. Nucl. Phys. **59**, 432 (2007).
[5] L.B. Wang *et al.*, Phys. Rev. Lett **93**, 142501 (2004).
[6] P. Mueller *et al.*, Phys. Rev. Lett **99**, 252501 (2008).
[7] M. Brodeur *et al.*, arXiv:1107.1684 (2011).
[8] I. Sick, Phys. Rev. C **77**, 041302(R) (2008).
[9] S.C. Pieper, Riv. Nuovo Cim. **031**, 709 (2008).
[10] E. Caurier and P. Navrátil, Phys. Rev. C **73**, 021302(R) (2006).
[11] N. Michel, *et al.*, Phys. Rev. Lett **89**, 042502 (2002); Phys. Rev. C **67**, 054311 (2003).
[12] T. Berggren, Nucl. Phys. A **109**, 265 (1968).
[13] N. Michel, W. Nazarewicz, and M. Płoszajczak, Phys. Rev. C **82**, 044315 (2010).
[14] G. Hagen, M. Hjorth-Jensen, and N. Michel, Phys. Rev. C **73**, 064307 (2006).
[15] G. Hagen *et al.*, Phys. Lett. B **656**, 169 (2007).
[16] Y. Suzuki and K. Ikeda, Phys. Rev. C **38**, 410 (1988).
[17] D.R. Thompson, M. LeMere, and Y.C. Tang, Nucl. Phys. A **268**, 53 (1977).
[18] N. Michel, W. Nazarewicz, and M. Płoszajczak, Phys. Rev. C **70**, 064313 (2004).
[19] A.T. Kruppa *et al.*, in preparation, (2011).
[20] J. Rotureau, *et al.*, Phys. Rev. Lett **97**, 110603 (2006); Phys. Rev. C **79**, 014304 (2009).
[21] S. Saito, Prog. Theor. Phys. **41**, 705 (1969).
[22] S.C. Pieper and R.B. Wiringa, Annu. Rev. Part. Sci **51**, 53 (2001); private communication (2011).
[23] J.L. Friar and J.W. Negele, Adv. Nucl. Phys. **8**, 219 (1975).
[24] W.-M Yao, *et al.*, J. Phys. G **33**, 1 (2006).
[25] J.L. Friar, J. Martorell, and D.W.L. Sprung, Phys. Rev. A **56**, 4579 (1997).
[26] G.F. Bertsch and H. Esbensen, Ann. Phys. (N.Y.) **209**, 327 (1991).
[27] K. Hagino and H. Sagawa, Phys. Rev. C **72**, 044321 (2005).
[28] D.R. Tilley *et al.*, Nucl. Phys. A **745**, 115 (2004).
[29] M. V. Zhukov *et al.*, Phys. Rep **231**, 151 (1993).
[30] Yu.Ts. Oganessian, V.I. Zagrebaev, and J.S. Vaagen, Phys. Rev. Lett **82** 4996, (1999).
[31] Y. Kikuchi *et al.*, Phys. Rev. C **81**, 044308 (2010).
[32] G.D. Alkhazov *et al.*, Phys. Rev. Lett **78**, 2313 (1997).
[33] A. Ong, J.C. Berengut, and V.V. Flambaum, Phys. Rev. C **82**, 014320 (2010).
[34] G. Papadimitriou, *et al.*, AIP Conf. Proc **1128**, 11 (2009); G. Papadimitriou, *et al.*, to be published.
[35] K. Bennaceur, J. Dobaczewski, and M. Płoszajczak, Phys. Lett. B **496** 154, (2000); Phys. Rev. C **60** 034308, (2000).
[36] M. Yamagami, Eur. Phys. J. A **25**, 569 (2005).
[37] M. Yamagami, Phys. Rev. C **72**, 064308 (2005).
[38] V. Rotival, and T. Duguet, Phys. Rev. C **79**, 054308 (2009); V. Rotival, K. Bennaceur, and T. Duguet, Phys. Rev. C **79**, 054308 (2009).
[39] K. Hagino and H. Sagawa, Phys. Rev. C **84**, 011303 (2011).
[40] K. Riisager, A.S. Jensen, and P. Møller, Nucl. Phys. A **548**, 393 (1992).